Robust Pseudocapacitive Na+ Intercalation Induced by Cobalt Vacancies at Atomically Thin Co1-xSe2/Graphene Heterostructure

Author

Dou, Yuhai, Yuan, Ding, Adekoya, David, Tian, Yuhui, Adekoya, Shanqing, Xu, Li, Zhang, Shanqing

Published

2021

Journal Title

Angewandte Chemie - International Edition

Version

Accepted Manuscript (AM)

DOI

10.1002/anie.202106857

A Journal of the Gesellschaft Deutscher Chemiker

Angewandte International Edition GDCh Chemie

www.angewandte.org

Accepted Article

Title: Robust Pseudocapacitive Na+ Intercalation Induced by Cobalt Vacancies at Atomically Thin Co1-xSe2/Graphene Heterostructure

Authors: Yuhai Dou, Ding Yuan, David Adekoya, Yuhui Tian, Shanqing Adekoya, Li Xu, and Shanqing Zhang

To be cited as: *Angew. Chem. Int. Ed.* 10.1002/anie.202106857

Link to VoR: https://doi.org/10.1002/anie.202106857

WILEY-VCH

10.1002/anie.202106857

WILEY-VCH

RESEARCH ARTICLE

Robust Pseudocapacitive Na^+ Intercalation Induced by Cobalt Vacancies at Atomically Thin $Co_{1-x}Se_2$/Graphene Heterostructure

Ding Yuan,[a] Yuhai Dou,*[a,b] Yuhui Tian,[a,d] David Adekoya,[a] Li Xu,[c] Shanqing Zhang*[a]

[a] Dr. D. Yuan, Dr. Y. Dou, Mr. Y. Tian, Dr. D. Adekoya, Prof. S. Zhang
Centre for Clean Environment and Energy
Griffith University
Gold Coast 4222, Australia
E-mail: y.dou@griffith.edu.au; s.zhang@griffith.edu.au
[b] Dr. Y. Dou
Shandong Institute of Advanced Technology
Jinan 250100, China
[c] Dr. L. Xu
Institute for Energy Research, School of Chemistry and Chemical Engineering, Key Laboratory of Zhenjiang
Jiangsu University
Zhenjiang 212013, China
[d] Mr. Y Tian
National Engineering Research Centre for Advanced Polymer Processing Technology, Zhengzhou University, Zhengzhou, 450002, China

Supporting information for this article is given via a link at the end of the document.

Abstract: Electronic structure engineering on electrode materials could bring in a new mechanism to achieve high energy and high power densities in sodium ion batteries. Herein, we design and create Co vacancies at the interface of atomically thin $CoSe_2$/graphene heterostructure and obtain $Co_{1-x}Se_2$/graphene heterostructure electrode materials that facilitate significant Na^+ intercalation pseudocapacitance. Density functional theory (DFT) calculation suggests that the Na^+ adsorption energy is dramatically increased, and the Na^+ diffusion barrier is remarkably reduced due to the introduction of Co vacancy. The optimized electrode delivers a superior capacity of 673.6 mAh g^{-1} at 0.1 C, excellent rate capability of 576.5 mAh g^{-1} at 2.0 C and ultra-long life up to 2000 cycles. Kinetics analysis indicates that the enhanced Na^+ storage is mainly attributed to the intercalation pseudocapacitance induced by Co vacancies. This work suggests that the creation of cation vacancy could bestow heterostructured electrode materials with pseudocapacitive Na^+ intercalation for high-capacity and high-rate energy storage.

Introduction

Lithium-ion batteries (LIBs) dominate the market of energy storage devices in the past two decades due to their high energy and power densities, long life and safety.[1] However, the high cost and scarce resource of lithium impede their further development. As a valid alternative, sodium-ion batteries (SIBs) have attracted increasing attention in recent years since they are more environmentally friendly and resource-abundant.[2] However, even though SIBs share a similar working principle with LIBs, the traditional electrodes that are effective in LIBs may not be suitable for SIBs.[3] Since the radius of Na^+ (1.02 Å) is 1.34 times larger than that of Li^+ (0.76 Å), the insertion of Na^+ normally results in sluggish kinetics and severe capacity fading.[4] Therefore, developing advanced electrode materials capable of reversibly accommodating Na^+ is highly desirable to alleviate the aforementioned issue.

Finding the right materials is the first step to build up efficient SIB electrodes. Chalcogenides are typically more reversible than oxides due to the relatively weaker metal-sulfur/selenium (M-S/Se) compared with metal-oxygen (M-O) bond, resulting in more kinetically favorable and higher first-cycle efficiency.[5] Moreover, carbonaceous materials like graphene are commonly incorporated to enhance the electrical conductivity and suppress the volume expansion.[6] Furthermore, morphology engineering plays a vital role in promoting the reversible storage of Na^+.[7] Especially, atomically thin metal chalcogenides possess high specific surface areas and thus could generate large interfacial areas when coupled with graphene, which dramatically shortens the ion diffusion pathway and creates highly accessible channels at the interface, facilitating surface redox pseudocapacitance and interfacial intercalation pseudocapacitance, respectively.[5, 8] The intercalation pseudocapacitance undergoes a faradaic storage mechanism, involving the ion intercalation/deintercalation on the same timescale as redox pseudocapacitance.[9]

A further step to fully unlock the power of atomically thin heterostructured electrodes is electronic structure engineering, which is important yet always underrated.[10] For the electrode of a single component, rational defect creation has been demonstrated to not only promote ion diffusion and charge transfer but also provide more active sites for reversible energy storage.[11] The role of the defects at the hetero-interface, however, has rarely been reported. Considering the intercalation pseudocapacitive behavior at the hetero-interface, we believe that cation vacancies should be a good choice since their presence could efficiently tune the adsorption energy and diffusion barrier of Na^+.[12] Especially, the presence of graphene (GE) in the heterostructure will facilitate the charge transfer process and enhance the role of cation vacancies at the interface.

Herein, as an example, we prepared atomically thin $CoSe_2$ nanobelt/graphene ($CoSe_2$/GE) heterostructure as an anode for SIB. Via a theory-guided approach, we induced and incorporated Co vacancies and consequently obtained $Co_{1-x}Se_2$/GE. Density functional theory (DFT) suggests that the Co vacancies could increase the Na^+ adsorption energy and decrease Na^+ diffusion

10.1002/anie.202106857

energy barrier, which dramatically enhance Na^+ storage performance. Such a theoretical estimation is confirmed by the remarkable specific capacity of 673.6 mAh g^{-1} at 0.1 C (1 C ≈ 494.36 mA g^{-1}), excellent rate capability of 576.5 mAh g^{-1} at 2.0 C and ultralong life up to 2000 cycles. The kinetic study on $CoSe_2$/GE and $Co_{1-x}Se_2$/GE concludes that the high-capacity and high-rate Na^+ storage are mainly contributed by the significant Na^+ intercalation pseudocapacitance at the $Co_{1-x}Se_2$/GE hetero-interface, which is consistent with the theoretical prediction.

Results and Discussion

Theoretical study of the roles of Co vacancies. To date, there have been very few studies regarding the effect of cation vacancies at the hetero-interface on Na^+ storage performance because of their high formation energy. Due to the lack of information on this topic, we will need to evaluate the role of Co vacancy theoretically in order to assure efficient reaction kinetic. DFT calculations were first performed to understand the role of Co vacancies at $Co_{1-x}Se_2$/GE interface in determining the Na^+ storage from an atomistic viewpoint. Figure 1a and b show the optimized structural models of $CoSe_2$/GE and $Co_{1-x}Se_2$/GE, respectively. The most stable Na adsorption positions at the interfaces of $CoSe_2$/GE (Figure 1c and Figure S1a) and $Co_{1-x}Se_2$/GE (Figure 1d and Figure S1b) were then identified and the calculated adsorption energies are 4.19 and 4.57 eV, respectively (Figure 1e). Therefore, the presence of Co vacancy at the interface leads to enhanced interaction between Na atom and heterostructure, which is beneficial for Na uptake.[13] The diffusion properties of Na at the hetero-interface were then investigated by the nudged elastic band method and the optimal diffusion paths for $CoSe_2$/GE and $Co_{1-x}Se_2$/GE were provided in Figure 1f&g and h&i, respectively. The diffusion energy barrier associated with this process for $Co_{1-x}Se_2$/GE is ~1.7 eV, which is much lower than that of ~3.7 eV for $CoSe_2$/GE (Figure 1j), indicating the dramatically enhanced diffusion kinetics and fast charge/discharge processes. Overall, our theoretical study suggests that the Co vacancies at the interface could not only create more active sites but also facilitate ion migration, enabling high capacity and high rate Na^+ storage for $Co_{2-x}Se_2$/GE.

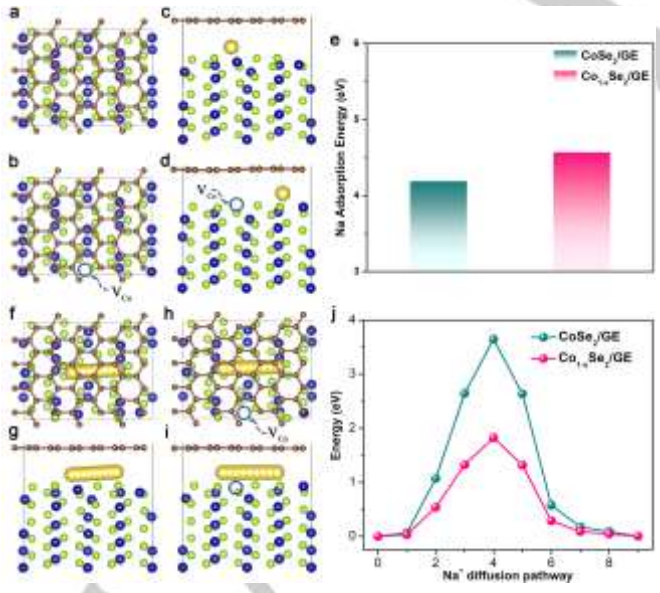

Figure 1. Theoretical study of the role of Co vacancies at the atomically thin interface in promoting the Na^+ storage performance. a, **b** Top views of the optimized $CoSe_2$/GE and $Co_{1-x}Se_2$/GE structures with green, blue and brown balls representing Se, Co and C atoms, respectively. **c**, **d** Side views of the most stable Na (yellow balls) adsorption positions at the interfaces of $CoSe_2$/GE and $Co_{1-x}Se_2$/GE. **e** Na adsorption energies. **f-i** Top and side views of Na diffusion pathways at the interfaces of $CoSe_2$/GE and $Co_{1-x}Se_2$/GE. **j** Na diffusion energy barriers.

Materials synthesis and structural characterization. To experimentally validate the proposed theory, atomically thin $Co_{1-x}Se_2$ nanobelt/GE heterostructure was prepared with the synthetic procedure shown in Figure 2a. Firstly, the $CoSe_2$ nuclei generated from Co and Se sources were coordinated with diethylenetriamine (DETA) under hydrothermal conditions. Then, atomically thin $CoSe_2$ nanobelts were assembled on the surface of graphene under the direction of DETA, forming DETA/$CoSe_2$/GE layered intermediates. After that, the obtained suspension was subjected to ultrasonication to separate DETA from $CoSe_2$. In this process, low-power ultrasonication leads to the formation of $CoSe_2$/GE, while high-power ultrasonication enables DETA to drag Co atoms out of the lattice,[14] resulting in the formation of $Co_{1-x}Se_2$/GE.

Figure 2b shows the high-angle annular dark-field scanning transmission electron microscopy (HAADF-STEM) image of $Co_{1-x}Se_2$/GE. Clearly, the $Co_{1-x}Se_2$ possesses an ultrathin nanobelt structure and is grown on the surface of graphene (inset of Figure 2b), indicating the strong coupling effect between them. The thickness of the heterostructure is ~4.6 nm according to the cross-sectional STEM image (Figure S2). Energy-dispersive X-ray spectroscopy (EDS) maps show that the Co, Se and C are homogeneously distributed throughout the heterostructure (Figure 2c), and the selected area electron diffraction (SAED)

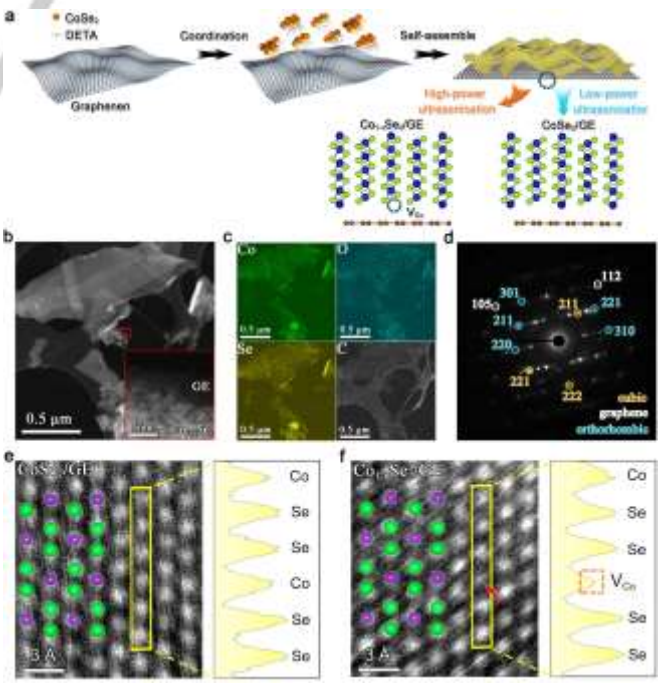

Figure 2. Synthesis and structural characterization of $CoSe_2$/GE and $Co_{1-x}Se_2$/GE. a Schematic illustration of the synthetic procedure. **b** STEM image of $Co_{1-x}Se_2$/GE with inset showing its growth on graphene. **c** Elemental maps of

Co, O, Se and C in $Co_{1-x}Se_2$/GE. **d** SAED pattern of $Co_{1-x}Se_2$/GE. **e** HAADF-STEM image of $CoSe_2$/GE, **f** HAADF-STEM image of $Co_{1-x}Se_2$/GE. The intensity profiles along the selected regions suggest the intact crystal structure of $CoSe_2$/GE and the presence of Co vacancy in $Co_{1-x}Se_2$/GE.

patterns reveal that the $Co_{1-x}Se_2$/GE is composed of cubic $CoSe_2$, orthorhombic $CoSe_2$ and graphene phases (some unspecified dots are probably attributed to the CoO_x impurities due to the limited solubility of Na_2SeO_3 in H_2O-DETA solvent). The intact orthorhombic crystal of $CoSe_2$/GE and the created Co vacancies in $Co_{1-x}Se_2$/GE are readily visible via high-resolution STEM (HR-STEM) images (Figure 2e and f). In addition, the intensity profile along the selected region also suggests the missed Co atom in $Co_{1-x}Se_2$/GE.

The phase structures of different electrodes were characterized by X-ray diffraction (Figure S3). The peaks are indexed to cubic $CoSe_2$ (JCPDS 09-0234), orthorhombic (JCPDS 53-0449) $CoSe_2$ and CoO_x impurities.[15] This was further confirmed by the Raman spectra (Figure S4). The peak located at 159 cm^{-1} is assigned to the stretching mode of Se-Se in $CoSe_2$,[16] while that at 204 cm^{-1} corresponds to the F_{2g} mode of CoO_x. In addition, there are two strong peaks in $CoSe_2$/GE and $Co_{1-x}Se_2$/GE located at 1350 and 1582 cm^{-1}, which are attributed to the D band and G band of graphene,[17] respectively.

Understanding the electronic structure induced by interface Co vacancies. The electronic structures of different electrodes were then studied via X-ray photoelectron spectroscopy (XPS), electron energy loss spectroscopy (EELS) and X-ray absorption fine structure spectroscopy (XAFS). The XPS survey spectra show the existence of Co, Se, C and O elements (Figure S5), which is consistent with the XRD and Raman results. The high-resolution Co 2p spectra were fitted by multiple Gaussian functions, representing the Co-Se, Co-O and satellites, respectively (Figure 3a). Notably, the Co-Se peaks of $Co_{1-x}Se_2$ and $Co_{1-x}Se_2$/GE shift to higher binding energies compared with those of $CoSe_2$ and $CoSe_2$/GE (Figure 3b), indicating the electron transfer from Co to Se induced by Co vacancies. Similarly, the positive shifts of Co $L_{2,3}$ edges of $Co_{1-x}Se_2$ and $Co_{1-x}Se_2$/GE from the EEL spectra were also detected (Figure 3c), originating from the changed electronic environment around Co vacancies.[18] The vacancy-tuned electronic structure was further analyzed by XAFS at the Co K edge. As shown in Figure 3d, the near-edge structure

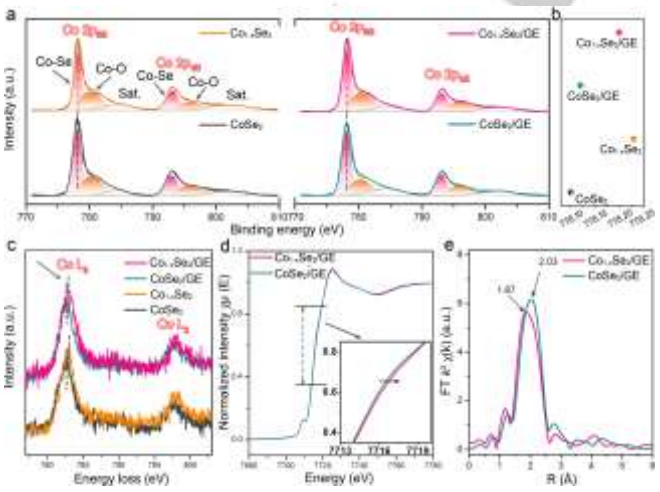

Figure 3. Electronic structure modulated by Co vacancies. a Co 2p XPS spectra of different electrodes. **b** Co–Se binding energy positions of different electrodes. **c** Co $L_{2,3}$-edge EEL spectra. **d** Co K-edge X-ray absorption near-edge structures of $CoSe_2$/GE and $Co_{1-x}Se_2$/GE. **e** Fourier transforms of Co K-edge extended X-ray absorption fine structures of $CoSe_2$/GE and $Co_{1-x}Se_2$/GE.

at Co K edge of $Co_{1-x}Se_2$/GE shows a slight positive shift compared to $CoSe_2$/GE, suggesting a higher oxidation state due to Co vacancies.[19] Moreover, the Fourier transform of Co K-edge extended X-ray absorption fine structure of $CoSe_2$/GE shows a main peak at R = 2.03 Å, representing the bond distance of the nearest Co-Se coordination. In comparison, the peak intensity of $Co_{1-x}Se_2$/GE decreases, attributing to the coordination missing induced by Co vacancies. In addition, the main peak of $Co_{1-x}Se_2$/GE shifts to 1.87 Å, which reflects the shortened Co-Se bond length due to the higher oxidation state of Co.[14]

Evaluation of Na^+ storage performance. Having proven the existence of Co vacancies at the interface and understood their role in tuning the electronic structure, we proceed to study their effect on Na^+ storage properties in Na half cells. The cyclic voltammetry (CV) of $Co_{1-x}Se_2$/GE was first conducted at a scan rate of 0.2 mV s^{-1} between 0.01 and 3.0 V (Figure 4a). Clearly, the cathodic scans show three reduction peaks at around 1.40, 1.09 and 0.54 V, which can be assigned to the intercalation, transition and conversion reactions between $Co_{1-x}Se_2$ and Na^+:[20]

$CoSe_2 + xNa^+ + xe^- \rightarrow Na_xCoSe_2$

$Na_xCoSe_2 + (2 - x)Na^+ + (2 - x)e^- \rightarrow Na_2Se + CoSe$

$CoSe + 2Na^+ + 2e^- \rightarrow Na_2Se + Co$

In anodic scans, only a strong oxidation peak appears at about 1.93 V, representing the desodiation process and the formation of $CoSe_2$:[21]

$Co + 2Na_2Se \rightarrow Na_xCoSe_2 + (4 - x)Na^+ + (4 - x)e^-$

$Na_xCoSe_2 \rightarrow xNa^+ + CoSe_2 + xe^-$

Notably, the reduction and oxidation peaks for the three cycles are well overlapped, implying the good reversibility and stability of $Co_{1-x}Se_2$/GE during the Na^+ insertion/extraction process. The complex Na^+ storage behavior of $Co_{1-x}Se_2$/GE was confirmed by the discharge/charge voltage profiles (Figure S6) and the proposed storage mechanism was verified by the HRSTEM images of $Co_{1-x}Se_2$/GE at fully discharged and charged states (Figure S7). Figure 4b shows the 20th discharge/charge profiles of different electrodes at 0.2 C. Clearly, the discharge capacities under 0.5 V follow a decreasing order of $Co_{1-x}Se_2$/GE (100.6) > $CoSe_2$/GE (59.7) > $Co_{1-x}Se_2$ (39.8) > $CoSe_2$ (36.3 mAh g^{-1}). Meanwhile, the $Co_{1-x}Se_2$/GE has the lowest charge platform among all the electrodes. The high low-voltage capacity and low charge platform of $Co_{1-x}Se_2$/GE could achieve high energy and power densities in full-cell applications.[22]

The rate performance and corresponding discharge/charge curves of different electrodes were evaluated at stepwise current densities of 0.1, 0.2, 0.5, 1.0, and 2.0 C (Figure 4c and Figure S8). The $Co_{1-x}Se_2$/GE delivers average discharge capacities of 673.6, 658.1, 637.1, 610.5 and 576.5 mAh g^{-1}, higher than 411.5, 401.0, 390.5, 372.0 and 342.9 mAh g^{-1} of $CoSe_2$/GE, respectively. They exhibit better rate capabilities than $Co_{1-x}Se_2$ and $CoSe_2$, respectively, and therefore both hetero-interface and Co vacancies are essential for the enhanced performance. Moreover, when the current density returns to 0.1 C, the capacity of $Co_{1-x}Se_2$/GE recovers to 655.6 mAh g^{-1}, indicating the remarkable reversibility and cyclability. Figure 4d demonstrates the cycling

performance at a current density of 0.2 C. The initial discharge capacities of $Co_{1-x}Se_2$/GE, $CoSe_2$/GE, $Co_{1-x}Se_2$, $CoSe_2$ and GE are 1155.9, 691.7, 563.6, 466.2 and 55.6 mAh g^{-1}, respectively, and the corresponding Coulombic efficiencies (CEs) are 57.8%, 58.1%, 60.2%, 46.2% and 55.6%, respectively. The relatively low CEs are due to the formed SEI layers on electrode surfaces.[23]

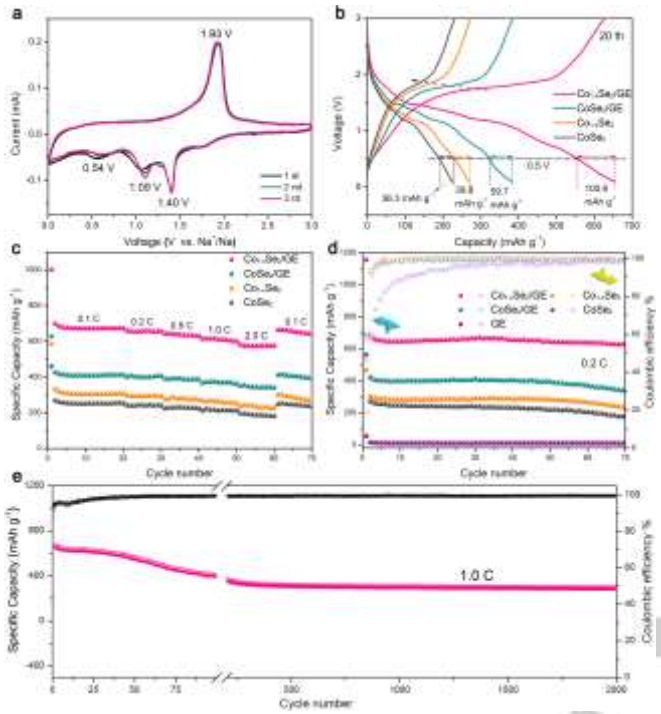

Figure 4. Sodium storage performance of different electrodes. a CV curves of $Co_{1-x}Se_2$/GE at 0.2 mV s^{-1} for three cycles. **b** Discharge–charge voltage profiles of different electrodes at 0.2 C at the 20th cycle. **c** Rate performance evaluated at stepwise current densities of 0.1, 0.2, 0.5, 1.0, and 2.0 C. **d** Cycle performance of different electrodes at 0.2 C. **e** Long-term cycling performance of $Co_{1-x}Se_2$/GE at 1.0 C.

After 70 cycles, the capacities of $Co_{1-x}Se_2$/GE, $CoSe_2$/GE, $Co_{1-x}Se_2$, $CoSe_2$ and GE maintain at 626.2, 340.4, 232.2, 176.3 and 9.7 mAh g^{-1}, respectively. Obviously, the capacity retention (compared with that of the 2nd cycle) of $Co_{1-x}Se_2$/GE is 91.0%, much higher than 80.9%, 77.2%, 64.9% of $CoSe_2$/GE, $Co_{1-x}Se_2$ and $CoSe_2$, respectively, further suggesting the high reversibility induced by Co vacancies at the interface.[12] To verify the importance of Co vacancies at the interface in improving the Na^+ storage property, long-term cycling performance at a high current density of 1.0 C was assessed. As shown in Figure 4e, the $Co_{1-x}Se_2$/GE electrode exhibits an ultra-long life up to 2000 cycles and could still deliver a high reversible capacity of 323.0 mAh g^{-1} with a high CE of 99.4%. It is noteworthy that the Na^+ storage property of $Co_{1-x}Se_2$/GE is among the best when compared to previously reported $CoSe_2$-based electrodes (Figure S1).

To understand the Na^+ storage mechanism, the reaction kinetics of different electrodes were analyzed by performing CV at varied scan rates from 0.2 to 100 mV s^{-1}. Figure 5a shows that both anodic and cathodic peaks become stronger and broader and the separation between them gradually increases with increasing scan rate, indicating an enhanced polarization at high scan rates. In respect of the CV measurements, a relationship exists between the peak current (i) and the scan rate (v):[24]

$$i = av^b \quad (1)$$

By plotting log(i) against log(v), the value of b can be obtained (Figure 5b). When the b-value approaches 0.5, the Na^+ storage is controlled by semi-infinite linear diffusion. By contrast, when it is close to 1.0, the Na^+ storage is dominated by a capacitive mechanism with fast reaction kinetics.[25] Take $Co_{1-x}Se_2$/GE as an example, the b-value in the range of 50–100 mV s^{-1} was calculated to be 0.74, implying a diffusion-controlled discharge/charge process, whereas that in the range of 0.2–20 mV s^{-1} was calculated to be 0.87, implying the capacitance-dominated electrochemical process. For $CoSe_2$/GE, $Co_{1-x}Se_2$ and $CoSe_2$, the capacitance-dominated storage behaviors locate in the ranges of 0.2–10, 0.2–2.0 and 0.2–1.0 mV s^{-1}, respectively. The relationship between normalized capacity and scan rate could be established. As shown in Figure 5c, the capacity of $Co_{1-x}Se_2$/GE is independent of the scan rate in the range of 0.2–20 mV s^{-1}, while those of $CoSe_2$/GE, $Co_{1-x}Se_2$ and $CoSe_2$ are in the ranges of 0.2–10, 0.2–2.0 and 0.2–1.0 mV s^{-1}, respectively. As a result, the capacity of $Co_{1-x}Se_2$/GE is more independent of the scan rate than other electrodes due to its dominated capacitive behavior,[26] which is consistent with the result in Fig. 5b.

To quantitatively determine the capacitive and diffusion-controlled contributions, the total current density (i) at a fixed potential can be separated into two parts:[27]

$$i = k_1v + k_2v^{1/2} \quad (2)$$

where k_1 and k_2 are parameters and k_1v and $k_2v^{1/2}$ represent the capacitive and diffusion-controlled contributions,[28] respectively. Figure 5d shows a typical example of the separated capacitive contribution of $Co_{1-x}Se_2$/GE at 1 mV s^{-1}, the ratio of which is estimated to be 90.1%. The capacitive contribution ratios of different electrodes at scan rates from 0.2 to 5 mV s^{-1} were also calculated and provided in Figure 5e. Obviously, they increase with increasing scan rate, suggesting that the diffusion-controlled reaction is suppressed under high scan rates. In addition, the capacitive contribution in $Co_{1-x}Se_2$/GE is the largest among all the electrodes, indicating the enhanced capacitive storage behavior induced by Co vacancies at the interface.[29] The electrochemical impedance spectroscopy was performed to understand the reaction kinetics of different electrodes. As shown in Figure 5f, based on the radius of the semi-circles in the Nyquist plots, $Co_{1-x}Se_2$/GE has the lowest charge transfer resistance, which agrees well with the CV kinetic analysis.

It is well known that the faradaic pseudocapacitance is several orders of magnitude higher than the electric double-layer capacitance,[30] and thus the capacitive contribution reported here originates mainly from a pseudocapacitive behavior. For atomically thin heterostructures, the pseudocapacitive storage is

10.1002/anie.202106857

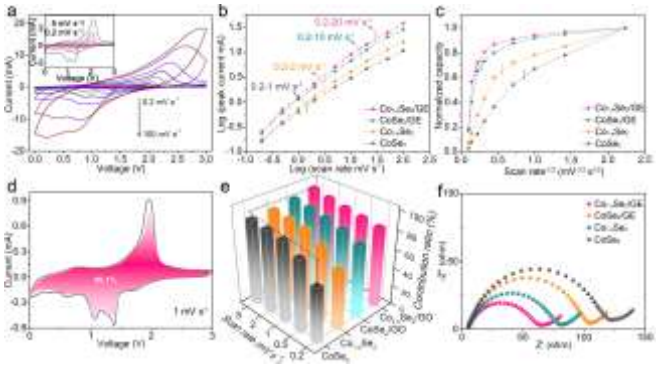

Figure 5. Reaction kinetics study of the Na^+ storage behavior. a CV curves of $Co_{1-x}Se_2$/GE at varied scan rates from 0.2 to 100 mV s^{-1}. **b** Log(i_{peak}) versus log(v). **c** Normalized capacity versus scan rate$^{-1/2}$. **d** Capacitive current separated from total current of $Co_{1-x}Se_2$/GE at 1 mV s^{-1} and calculated capacitive contribution. **e** Capacity contribution ratios at 0.2, 0.5, 1, 2, 5 mV s^{-1}. **f** Nyquist plots at fully discharged states.

composed of surface redox pseudocapacitance and interfacial intercalation pseudocapacitance.[31] The creation of Co vacancies on the surface of $Co_{1-x}Se_2$/GE will not lead to the obvious change in the surface redox pseudocapacitance due to the conversion storage mechanism.[32] Therefore, the high-capacity and high-rate storage property of $Co_{1-x}Se_2$/GE compared to $CoSe_2$/GE is mainly attributable to the boosted intercalation pseudocapacitance. According to the experimental results and theoretical calculations, the high Na^+ adsorption capacity and fast Na^+ diffusion kinetics induced by Co vacancies at $Co_{1-x}Se_2$/GE interface should be the main reason of the greatly enhanced intercalation pseudocapacitance.

Conclusion

To summary, through a theory-guided approach, we discover a remarkable Na^+ intercalation pseudocapacitive energy storage mechanism at the interface of $Co_{1-x}Se_2$/GE with Co vacancies. The Co vacancies enhance Na^+ adsorption energy and reduce Na^+ diffusion barrier, resulting in high storage capacity and fast electrode kinetics. As a result, the as-prepared electrode delivers high specific capacity, excellent rate capability and ultralong cycle life, significantly outperforming reported $CoSe_2$-based electrodes. This work could open up a new way for the design of high-energy and high-power electrodes by stimulating the pseudocapacitive storage behavior via rational defect engineering.

Acknowledgements

This work was financially supported by an Australian Research Council (ARC) Discovery Project (DP210103266) and an ARC Discovery Early Career Researcher Award (DE210101102). Ding Yuan was funded by a Completion Assistance Scholarship and a Publication Assistance Scholarship from Griffith University. The authors also acknowledge the National Computational Infrastructure National Facility systems at the Australian National University and the PAWSEY Supercomputing Centre located in Western Australia for providing computational resources.

Keywords: Atomically thin • heterostructure • cobalt vacancies • Intercalation pseudocapacitance • sodium-ion batteries

[1] Z. Sun, X.-L. Wu, J. Xu, D. Qu, B. Zhao, Z. Gu, W. Li, H. Liang, L. Gao, Y. Fan, K. Zhou, D. Han, S. Gan, Y. Zhang, L. Niu, *Small* **2020**, *16*, 1907670.

[2] Y. Fang, X.-Y. Yu, X. W. Lou, *Adv. Mater.* **2018**, *30*, 1706668.

[3] J. Yang, H. Gao, S. Men, Z. Shi, Z. Lin, X. Kang, S. Chen, *Adv. Sci.* **2018**, *5*, 1800763.

[4] a) P. Ge, H. Hou, S. Li, L. Huang, X. Ji, *ACS Appl. Mater. Inter.* **2018**, *10*, 14716-14726; b) B. Li, Y. Liu, X. Jin, S. Jiao, G. Wang, B. Peng, S. Zeng, L. Shi, J. Li, G. Zhang, *Small* **2019**, *15*, 1902881; c) Q. Wei, R. H. DeBlock, D. M. Butts, C. Choi, B. Dunn, *Energy Environ. Mater.* **2020**, *3*, 221-234.

[5] M. Yousaf, Y. Chen, H. Tabassum, Z. Wang, Y. Wang, A. Y. Abid, A. Mahmood, N. Mahmood, S. Guo, R. P. S. Han, P. Gao, *Adv. Sci.* **2020**, *7*, 1902907.

[6] a) H. Tabassum, C. Zhi, T. Hussain, T. Qiu, W. Aftab, R. Zou, *Adv. Energy. Mater.* **2019**, *9*, 1901778; c) Q. Yu, B. Jiang, J. Hu, C.-Y. Lao, Y. Gao, P. Li, Z. Liu, G. Suo, D. He, W. Wang, G. Yin, *Adv. Sci.* **2018**, *5*, 1800782.

[7] a) G. Zhang, K. Liu, S. Liu, H. Song, J. Zhou, *J. Alloy. Compd.* **2018**, *731*, 714-722; b) G. Wei, Y. Jiang, J. Zhou, Z. Wang, Y. Huang, M. Xie, F. Wu, Energy Storage Science and Technology **2020**, *9*, 1318-1326.

[8] a) B. Guo, Q. Ma, L. Zhang, T. Yang, D. Liu, X. Zhang, Y. Qi, S.-J. Bao, M. Xu, *Chem. Eng. J.* **2020**, *413,* 127521. b) X. Chang, T. Huang, J. Yu, J. Li, J. Wang, Q. Wei, *Batteries & Supercaps* **2021**, https://doi.org/10.1002/batt.202100043.

[9] T. Brezesinski, J. Wang, S. H. Tolbert, B. Dunn, *Nat. Mater.* **2010**, *9*, 146-151.

[10] a) D. Yuan, D. Adekoya, Y. Dou, Y. Tian, H. Chen, Z. Wu, J. Qin, L. Yu, J. Zhang, X. Liu, S. X. Dou, S. Zhang, *J. Energy Chem.* **2021**, *62*, 281-288; b) D. Yuan, Y. Dou, L. Xu, L. Yu, N. Cheng, Q. Xia, L. Hencz, J. Ma, S. X. Dou, S. Zhang, *J. Mater. Chem. A.* **2020**, *8,* 13443-13451. c) F. Zhao, Y. Guo, X. Zhou, W. Shi, G. Yu, *Nat. Rev. Mater*. **2020**, *5*, 388-401.

[11] a) S. Wang, L. Pan, J. J. Song, W. Mi, J. J. Zou, L. Wang, X. Zhang, *J. Am. Chem. Soc.* **2015**, *137*, 2975-2983; b) Z. Y. Yu, Y. Duan, J. D. Liu, Y. Chen, X. K. Liu, W. Liu, T. Ma, Y. Li, X. S. Zheng, T. Yao, M. R. Gao, J. F. Zhu, B. J. Ye, S. H. Yu, *Nat. Commun.* **2019**, *10*, 2799.

[12] P. Xiong, X. Zhang, F. Zhang, D. Yi, J. Zhang, B. Sun, H. Tian, D. Shanmukaraj, T. Rojo, M. Armand, R. Ma, T. Sasaki, G. Wang, *ACS Nano* 2018, 12, 12337-12346.

[13] X. Li, K. Li, S. Zhu, K. Fan, L. Lyu, H. Yao, Y. Li, J. Hu, H. Huang, Y.-W. Mai, J. B. Goodenough, *Angew. Chem. Int. Ed*. **2019**, *58*, 6239-6243.

[14] Y. Liu, H. Cheng, M. Lyu, S. Fan, Q. Liu, W. Zhang, Y. Zhi, C. Wang, C. Xiao, S. Wei, B. Ye, Y. Xie, *J. Am. Chem. Soc.* **2014**, *136*, 15670-15675.

[15] a) Y. Dou, C.-T. He, L. Zhang, H. Yin, M. Al-Mamun, J. Ma, H. Zhao, *Nat. Commun.* **2020**, *11*, 1664; b) O. B. Ayodele, *Sci. Rep.* **2017**, *7*, 10008; c) X. Zhang, J. Zhou, Y. Zheng, D. Chen, *J. Power Sources.* **2019**, *439*, 227112.

[16] a) A. Ali, W.-C. Oh, *J. Korean Ceram. Soc* **2017**, *54*, 205-210; b) H. Yue, D. Yang, B. Yu, Y. Lu, W. Zhang, Y. Chen, *J. Mater. Sci.* **2019**, *54*, 14123-14133.

[17] M. S. Jo, J. S. Lee, S. Y. Jeong, J. K. Kim, Y. C. Kang, D. W. Kang, S. M. Jeong, J. S. Cho, *Small* **2020**, *16*, 2003391.

[18] Z. L. Wang, J. S. Yin, Y. D. Jiang, *Micron* **2000**, *31*, 571-580.

[19] a) X. Zheng, X. Han, Y. Cao, Y. Zhang, D. Nordlund, J. Wang, S. Chou, H. Liu, L. Li, C. Zhong, Y. Deng, W. Hu, *Adv. Mater.* **2020**, *32*, 2000607; b) L. Zhuang, Y. Jia, H. Liu, X. Wang, R. K. Hocking, H. Liu, J. Chen, L. Ge, L. Zhang, M. Li, C. L. Dong, Y. C. Huang, S. Shen, D. Yang, Z. Zhu, X. Yao, *Adv. Mater.* **2019**, *31*, 1805581.

[20] Y. Pan, X. Cheng, M. Gao, Y. Fu, J. Feng, L. Gong, H. Ahmed, H. Zhang, V. S. Battaglia, *ACS Appl. Mater. Inter.* **2020**, *12*, 33621-33630.

[21] J. Sun, D. Ji, H. Ye, B. Yu, Y. Wang, S. Ramakrishna, L. Lu, *Cell Rep. Phys. Sci.* **2020**, *1*, 100082.

[22] Y. Jiang, G. Zou, H. Hou, J. Li, C. Liu, X. Qiu, X. Ji, *ACS Nano* **2019**, *13*, 10787-10797.

10.1002/anie.202106857

[23] D. Chen, G. Chen, J. Pei, Y. Hu, Z. Qin, J. Wang, F. Wu, *ChemElectroChem* **2017**, *4*, 2158-2163.

[24] Z. Ali, T. Tang, X. Huang, Y. Wang, M. Asif, Y. Hou, *Energy Storage Mater.* **2018**, *13*, 19-28.

[25] J. Jin, Y. Zheng, L. B. Kong, N. Srikanth, Q. Yan, K. Zhou, *J. Mater. Chem. A.* **2018**, *6*, 15710-15717.

[26] B. Chen, L. Yang, X. Bai, Q. Wu, M. Liang, Y. Wang, N. Zhao, C. Shi, B. Zhou, C. He, *Small* **2021**, *17*, 2006824.

[27] C. An, Y. Yuan, B. Zhang, L. Tang, B. Xiao, Z. He, J. Zheng, J. Lu, *Adv. Energy Mater.* **2019**, *9*, 1900356.

[28] B. Sun, S. Lou, W. Zheng, Z. Qian, C. Cui, P. Zuo, C. Du, J. Xie, J. Wang, G. Yin, *Nano Energy* **2020**, *78*, 105366.

[29] Z. Yi, Y. Qian, J. Tian, K. Shen, N. Lin, Y. Qian, *J. Mater. Chem. A.* **2019**, *7*, 12283-12291.

[30] S. R. Taylor, E. Gileadi, *Corrosion* **1995**, *51*, 664-671.

[31] a) C. Chen, Y. Wen, X. Hu, X. Ji, M. Yan, L. Mai, P. Hu, B. Shan, Y. Huang, *Nat. Commun.* **2015**, *6*, 6929. b) C. An, Y. Yuan, B. Zhang, L. Tang, B. Xiao, Z. He, J. Zheng, J. Lu, *Adv. Energy Mater.* **2019**, *9*, 1900356.

[32] K. Zhang, M. Park, L. Zhou, G.-H. Lee, W. Li, Y.-M. Kang, J. Chen, *Adv. Funct. Mater.* **2016**, *26*, 6728-6735.

10.1002/anie.202106857

Entry for the Table of Contents

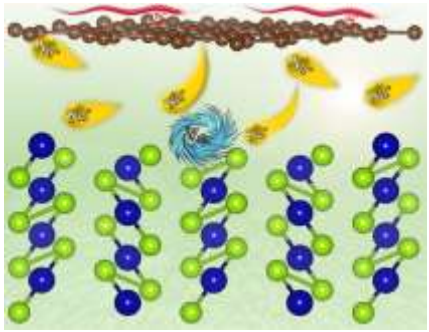

The Co vacancies (V_{Co}) at the interface of $Co_{1-x}Se_2$/GE afford the strong adsorption of Na^+ and low Na^+ diffusion energy barrier to facilitate rapid intercalation/deintercalation of Na^+ ions and incur remarkable pseudocapacitance. The as-prepared $Co_{1-x}Se_2$/GE-based sodium ion batteries deliver high specific/rate capacity performance and exceptional cycling performance.